Structural effects due to the incorporation of Ar atoms in the lattice of ZrO2 thin films prepared by ion beam assisted deposition

Holgado, J.P.; Escobar Galindo, R.; van Veen, A.; Schut, H.; de Hosson, J.T.M.; Gonzalez-Elipe, A.R.

Published in:
Nuclear Instruments & Methods in Physics Research Section B-Beam Interactions with Materials and Atoms

DOI:
10.1016/S0168-583X(02)00695-X

ELSEVIER

Nuclear Instruments and Methods in Physics Research B 194 (2002) 333–345

NIM B
Beam Interactions with Materials & Atoms

www.elsevier.com/locate/nimb

Structural effects due to the incorporation of Ar atoms in the lattice of ZrO_2 thin films prepared by ion beam assisted deposition

J.P. Holgado [a], R. Escobar Galindo [b], A. van Veen [b], H. Schut [b], J.Th.M. de Hosson [c], A.R. González-Elipe [a,*]

[a] *Instituto de Ciencia de Materiales de Sevilla (CSIC/Universidad de Sevilla) and Dpto. de Química, Inorgánica Univ. Sevilla., Av. Americo Vespucio S/N, E-41092 Sevilla, Spain*

[b] *Interfaculty Reactor Institute, Defects in Materials, Delft University of Technology, Mekelweg 15, 2629 JB Delft, The Netherlands*

[c] *Materials Science Center, University of Groningen, Nijenborgh 4, 9747 AG Groningen, The Netherlands*

Received 4 October 2001; received in revised form 27 January 2002

Abstract

Two sets of ZrO_2 thin films have been prepared at room temperature by ion beam induced chemical vapour deposition and subsequently annealed up to 1323 K. The two sets of samples have been prepared by using either O_2^+ or mixtures of ($O_2^+ + Ar^+$) ions for the decomposition of a volatile metallorganic precursor of zirconium. The structure and microstructure of these two sets of samples have been determined by means of X-ray diffraction, Fourier transform infrared spectroscopy and positron beam analysis (PBA). The samples were very compact and dense and had a very low-surface roughness. After annealing in air at $T \geqslant 573$ K both sets of films were transparent and showed similar refraction indexes.

For the ($O_2^+ + Ar^+$)-ZrO_2 thin films it is shown by X-ray photoelectron spectroscopy and Rutherford back scattering that a certain amount of incorporated Ar (5–6 at.%) remains incorporated within the oxide lattice. No changes were detected in the amount of incorporated Ar even after annealing at $T = 773$ K. For higher annealing temperatures ($T > 1073$ K), the amount of Ar starts to decrease, and at $T = 1223$ K only residual amounts of Ar (<0.4%) remain within the lattice. It has been found that as far as Ar atoms remain incorporated within the ZrO_2 network, the (O_2^+–Ar^+)-ZrO_2 films present a cubic/tetragonal phase. When the amount of "embedded" Ar decreases, the crystalline phase reverts to monoclinic, the majority phase observed for the (O_2^+)-ZrO_2 films after any annealing treatments.

The microstructure of the films after different annealing treatments has been investigated by PBA. The presence of Ar ions and the initial amorphous state of the layers were detected by this technique. An increase of the open volume was observed after annealing up to 773 K in both sets of samples. For higher annealing temperatures the samples showed a progressive crystallisation resulting in a decrease of the open volume. During this sintering the samples without embedded Ar present a higher concentration of open volume defects. After the release of Ar occurs ($T \geqslant 1223$ K) both samples approach to a similar defect free state.

* Corresponding author. Fax: +34-954-460-665.
E-mail address: agustin@cica.es (A.R. González-Elipe).

PII: S0168-583X(02)00695-X

The incorporation of Ar within the ZrO_2 thin film structure, is proposed as the main factor contributing to the stabilisation of the cubic/tetragonal phase of ZrO_2 at room temperature.

Keywords: Chemical vapour deposition; Ion bombardment; Thin film; Positron annihilation; Phase transformation; Ion assisted deposition; ZrO_2

1. Introduction

Among many other applications, such as optical coatings [1], buffer layers for growing superconductors [2], heat resistant coatings [3], oxygen sensors [5], etc. ..., ZrO_2 thin films have attracted great attention because of their properties as ion conductors [4], to be used in the so-called solid oxide fuel cells (SOFCs) [5]. For all these applications, and specially in the case of SOFCs, it is generally desirable to obtain the tetragonal or cubic phase of zirconia. It is known that although the tetragonal phase of ZrO_2 is unstable at room temperature, it can be stabilised by doping with cations such as Y^{3+}, Ca^{2+}, etc. [6], or by decreasing the particle size of the crystalline domains [7]. The synthesis of ZrO_2 or ZrO_2 doped thin films (i.e. ZrO_2-M) has been attempted by many different methods including spray deposition [8], chemical vapour deposition (CVD) [9], electron evaporation [10], and other methods [11].

Very compact ZrO_2(M) thin films can be prepared by ion beam assisted deposition procedures (IBAD) [12] that involve the bombardment of the growing film with low-energy ion beams (i.e. generally $E \geqslant 1000$ eV), usually O_2^+, Ar^+ or mixtures of both. By these methods, it is very common to observe the appearance of different crystallographic effects, such as amorphisation or the preferential growth of some crystallographic planes [13,14] that are attributed to the influence of the bombardment with low-energy ions [15]. Martin [16] has shown that monoclinic to tetragonal phase transformations can be induced in ZrO_2 thin films by bombardment with Ar^+ ions of relatively low energy. For bulk ZrO_2 the effect of high-energy Ar^+ bombardment in inducing crystallographic transformations and the stabilisation of the cubic/tetragonal phase is well known [17]. In most cases an implicit explanation of this type of monoclinic to cubic/tetragonal transformation relies on the assumption that ballistic interactions between the energetic ions and the target atoms are responsible for the phase change. The results presented in the present paper do not exactly support such an explanation based on energetic effects, but rather emphasise the role of Ar embedded within the ZrO_2 thin film in producing the stabilisation of the cubic/tetragonal phase. We compare the structural evolution of ZrO_2 thin films prepared by ion beam induced chemical vapour deposition (IBICVD) by using either O_2^+ or mixed $O_2^+ + Ar^+$ ion beams. In the latter case the cubic/tetragonal phase is stabilised upon annealing, as long as Ar atoms remain incorporated within the thin films. In a previous paper [18] we have studied in detail how the texture, morphology and optical properties of the resulting films are affected by the use of Ar^+ ions. The first motivation for the present paper is then to highlight how the presence of incorporated Ar may stabilise the cubic/tetragonal structure of zirconia acting in a similar way than "doping" cations such as Y^{3+}, Ca^{2+}, etc. and to provide an analysis of the evolution of structural defects in the samples upon annealing, as determined by positron beam analysis (PBA).

2. Experimental

Thin films have been prepared by IBICVD [19]. This method consists of the decomposition of a volatile metallic precursor by means of an ion beam. Further details about the method as applied to the synthesis of oxides and nitrides can be found in previous publications [19–21].

Zirconium tetra ter-butoxide, $Zr(OBu^t)_4$ has been used as precursor. Typical partial pressure

during deposition was 4×10^{-5} mbar. O_2^+ or mixtures of $O_2^+ + Ar^+$ ions, accelerated to 400 eV, were supplied by an "IQP" broad ion source. $O_2 + Ar$ mixtures with a molar ratio 10:1 were used for preparation of Ar-incorporated samples. A beam current of around 40 $\mu A\,cm^{-2}$ was measured at the sample holder during deposition. The total pressure in the chamber during deposition was 5×10^{-4} mbar. Under these conditions a growth rate of approximately 2.0 $nm\,min^{-1}$ was measured with a quartz crystal monitor at the sample position.

Silicon (1 0 0) wafers and fused quartz have been used as substrates for preparation of the samples.

X-ray diffraction (XRD) spectra were recorded by using the Cu Kα radiation with a Siemens D5000 diffractometer. An incidence angle of 0.5° was chosen to increase the sensitivity.

IR spectra were obtained with a Nicolet spectrometer at 8 cm^{-1} resolution for samples prepared on Si wafers. The silicon substrate was partially transparent to infrared radiation showing a small feature at 609 cm^{-1}.

Annealing of the samples in air was carried out in a conventional atmospheric furnace, using a linear heating ramp of 10 $K\,min^{-1}$. At the end of the ramp the selected final temperature was kept for 3 h followed by cooling down slowly.

Rutherford back scattering (RBS) spectra were recorded with a tandem ion accelerator (Pelletron 9SH-2 from NEC) at the Centro Nacional de Aceleradores (CNA) in Seville. Alpha particles of 2.021 MeV and usual settings of scattering angle and detector geometry were used for recording of spectra. The data acquisition was done with a total sample charge of 5 μC. Simulations of composition profiles have been done with the RUMP program code [22].

X-ray photoelectron spectroscopy (XPS) was carried out using an ESCALAB 210 spectrometer working in pass energy constant mode with a value of 50 eV. The surface concentration of the elements was determined by measuring the peak areas and correcting by the appropriate sensitivity values.

The PBA was performed using the Delft variable energy positron beam (VEP) [23]. The positrons were injected in the samples with energies between 100 eV and 25 keV. Annihilation of positrons with electrons results, in the center-of-mass system, in the emision of two collinear photons of 511 keV each. In the laboratory frame the non-zero momentum of the positron-electron pair causes an energy shift of the photons. This results in a broader energy distribution, called Doppler broadening of the annihilation radiation (DBAR) around the 511 keV peak. This broadened energy spectrum is characterised by two parameters: S and W. The S (shape) parameter is defined as the ratio between the central area and the total area of the annihilation photopeak. This parameter reflects the annihilation of positrons with valence electrons (low-momentum electrons). In general, a high value of S indicates positron annihilation in open volume defects. If the material allows the formation of a Positronium state (Ps) this will contribute to the DBAR with a narrow component because of the low-intrinsic moment of the para-positronium. A second useful parameter for the analysis of DBAR is the W (wing) parameter, which reflects the positron annihilation with high-momentum electrons (core electrons). The W-parameter is sensitive to changes in the chemical environment. Both parameters can be combined in S–W maps with a third variable (e.g. the implantation energy, temperature or strain) as a running parameter. These maps are useful to trace positron trapping in, e.g., layers as in the samples described in this work. The data was analysed with the variable energy positron fit (VEPFIT) program [24]. The samples studied here are modelled by a number of stacked slabs. Each of these slabs is characterised by a thickness (d_i), S_i and W_i parameters, and a positron diffusion length (L_i). The measured $S(E)$ and $W(E)$ as a function of the implantation energy E, are a sum of the characteristic S_i and W_i values of the trapping layers (cluster points) weighted by the fraction of positrons trapped in each layer $f_i(E)$. The spectra were recorded with a single Ge solid-state detector. All experiments were carried out at room temperature under a vacuum of about 10^{-6} Pa. The values of S and W parameters are normalised with respect to the S and W values for a crystal Si substrate ($S_{Si} = 0.58$, $W_{Si} = 0.031$).

3. Results

3.1. Chemical composition

The determination of the chemical composition of the zirconia films was done by XPS and RBS. The photoelectron spectra of both set of samples, prepared by using O_2^+ or ($O_2^+ + Ar^+$) ions, were typical for a ZrO_2 stoichiometry. Besides a carbon peak, which is easily removed by bombardment with Ar^+ or O_2^+ (and thus proving that it is due to contamination by exposure to air), no other contaminant species were detected at the surface of samples. In the case of ($O_2^+ + Ar^+$)-ZrO_2 samples, Ar2p and Ar2s peaks could be detected in the photoelectron spectra of the films. Their intensities were equivalent to an atomic percentage of approximately 5–6%, a value that did not change after cleaning by sputtering with O_2^+ ions of 3 keV energy. The samples were also analysed by RBS to obtain a more precise quantitative determination of the amount of Ar present in the samples, as well as an evaluation of the chemical composition profile for the whole film thickness. Fig. 1 shows experimental and theoretically calculated spectra for the as prepared ($O_2^+ + Ar^+$)-ZrO_2 and O_2^+-ZrO_2 samples. The right of this figure shows, in an enlarged scale, the Ar region of some spectra corresponding to ($O_2^+ + Ar^+$)-ZrO_2 samples annealed at increasing temperatures up to 1423 K. In the (O_2^+)-ZrO_2 and (O_2^+–Ar^+)-ZrO_2 samples the O/Zr ratio was close to 2.0, although a slightly smaller ratio (i.e. $\cong$1.95–2.00) was obtained for the as prepared (O_2^+–Ar^+)-ZrO_2 thin film. For these samples, Ar ($\approx$5–6 at.%) is found to be distributed homogeneously over the whole film thickness even after their annealing at temperatures as high as 873 K. After annealing of the samples at $T > 773$ K the concentration of Ar within the film decreases. It is found that at 1073 K only $\approx$3% of Ar is still retained by the thin film, and that a smaller concentration is observed at its surface. After annealing at 1323 K, only a 0.5 at.% of Ar is present, with an even lower concentration at the surface of the thin film. These results indicate that annealing treatments above 1073 K provoke a progressive loss of the Ar incorporated within the structure of zirconia films. This loss is more pronounced from the topmost surface layers of the ZrO_2 thin films.

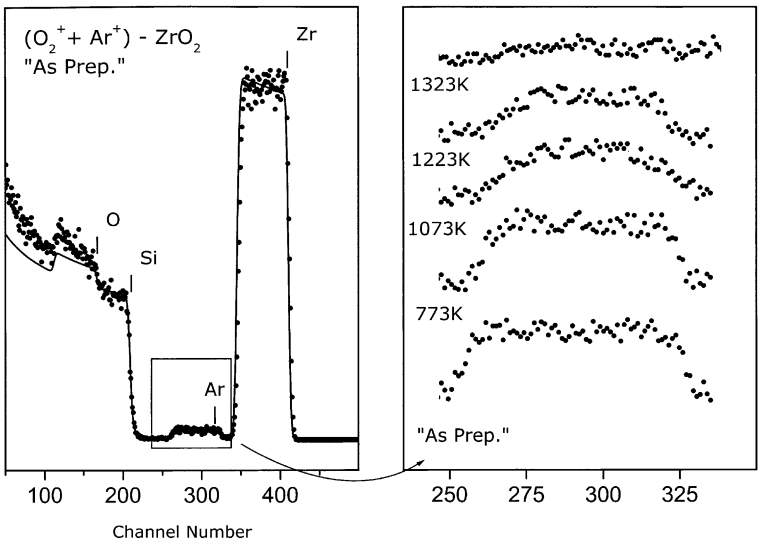

Fig. 1. Experimental and simulated RBS spectra of the ($O_2^+ + Ar^+$)-ZrO_2 sample. The inset shows, in an enlarged scale, the region corresponding to embedded Ar after annealing treatments at indicated temperatures.

3.2. Crystallographic structure

Fig. 2 shows XRD patterns for (O_2^+)-ZrO_2 thin films prepared at 298 K and after annealing at increasingly higher temperatures up to 1323 K.

For comparison, the reference patterns of the most intense peaks of the different phases of zirconia are included in the top part of the figure. The spectrum of the as prepared (O_2^+)-ZrO_2 sample reveal the existence of at least two phases: monoclinic and cubic and/or tetragonal. It should be remarked here that the diffractograms corresponding to these two phases present a series of peaks with very similar intensity and with very close positions. Due to the large width of the peaks obtained in the diagram of the thin film and the possible displacement of the positions of the peaks respect to those of the pure phases due to stress and strain effects, even a careful analysis of the positions of the peaks do not permit to discriminate between the cubic and/or the tetragonal phase of zirconia in the thin film. Thus, in the following discussion a mention to cubic/tetragonal phase should always be taken as a possible existence of any of those phases or a mixture of both. Annealing at $T < 773$ K leads to a relative increase of the monoclinic phase, although only a small change in the width of the peaks is observed in this range of temperatures. By contrast, when the samples are annealed at higher temperatures ($T > 873$ K), a drastic decrease is observed in the intensity of the peaks associated with the cubic/tetragonal phase. These peaks practically disappear from the spectrum when the film was annealed at $T \geqslant 1223$ K. This annealing treatment induces an increase in the height and a decrease in the width of the peaks corresponding to the monoclinic phase (Table 1). For the whole temperature range of annealing, the relative intensity of the peaks of the monoclinic phase was far from the ratio observed in a single crystal, thus indicating the preferential growth in the films of some crystallographic planes (cf. Table 1).

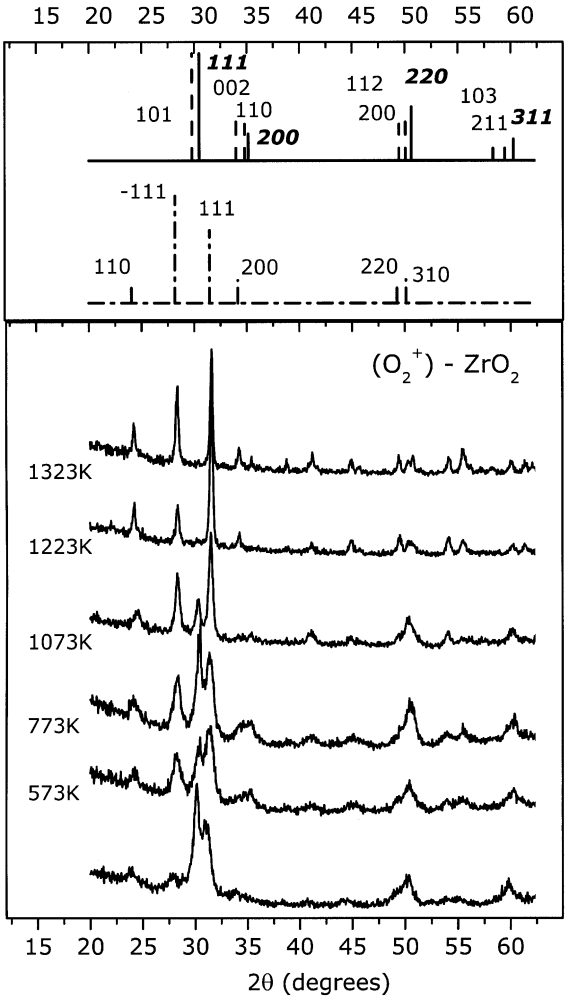

Fig. 2. XRD patterns of O_2^+-ZrO_2 thin film for the as prepared samples and after annealing treatments at indicated temperatures. The patterns of the most intense peaks of monoclinic (bottom), cubic (top, full line) and tetragonal (top, dashed line) phases of zirconia are included for comparison.

XRD patterns for $(O_2^+ + Ar^+)$-ZrO_2 films prepared at 298K and subsequently annealed at increasingly higher temperatures up to 1323 K are presented in Fig. 3. The XRD pattern of the "as deposited" $(O_2^+ + Ar^+)$-ZrO_2 films depicts only two broad features at diffraction angles which suggest the existence of a badly ordered cubic or tetragonal structure of ZrO_2. Again, the width of the peaks makes it very difficult to discriminate between these two phases, and in the following discussion it should always be kept in mind the possible existence of either cubic/tetragonal phases or even a mixture of both. Although the position of the diffraction lines is consistent with those of the cubic/tetragonal phases, the observed intensities are far

Table 1
Normalised intensity, referred to most intense peak of each phase and FWHM (in brackets) of the most significant peaks appearing in XRD diagrams of Fig. 2 for (O_2^+)-ZrO_2 samples after indicated annealing treatments

Temperature	Monoclinic			Cubic/tetragonal		
	(1 1 0)	(−1 1 1)	(1 1 1)	(1 1 1)	(2 2 0)	(3 1 1)
300 K	18 (0.98)	18 (0.90)	100 (0.82)	100 (0.92)	–	–
573 K	19 (0.85)	45 (0.83)	100 (0.82)	100 (0.88)	–	–
773 K	21 (0.75)	58 (0.75)	100 (0.62)	100 (0.81)	–	–
1073 K	14 (0.72)	58 (0.57)	100 (0.39)	100 (0.40)	–	–
1223 K	18 (0.32)	21 (0.32)	100 (0.26)	–	–	–
1323 K	25 (0.25)	63 (0.29)	100 (0.23)	–	–	–
Single crystal	25	100	70	100	50	20

from reference patterns. In particular, the high intensity of the peak at $2\theta \cong 59.4°$, indicates a preferential growth of the film according to the corresponding (3 1 1) planes of the cubic phase and/or the (2 1 1) plane of the tetragonal phase. The preferential growth of planes with high Miller indices has been recently reported by us for Fe_2O_3 thin films prepared also by IBICVD [25]. Such a preferential growth was related with the presence of Ar embedded in the structure.

By annealing these zirconia samples at $T \geqslant 573$ K the diffraction pattern changed. The maximum of the peak at $2\theta = 59.4°$ becomes slightly broader with a small asymmetry at higher diffraction angles. Simultaneously, a broad feature appears at $2\theta = 33$–$35°$. The comparison of these structures with the lines corresponding to the reference pattern of the bulk material, suggests the existence of a badly ordered cubic/tetragonal phase of zirconia in the as prepared samples and their progressive ordering or restructuring with the annealing treatments.

A significant change in the diffraction diagram of the $(O_2 + Ar^+)$-ZrO_2 samples is observed after annealing at $T = 1073$ K. In this case the peak corresponding to planes (3 1 1) is still the most intense, but becomes narrower (cf. Table 2). In this diagram peaks at ≈33–35° are now clearly visible, probably corresponding to some diffraction planes of the cubic/tetragonal phase of zirconia and/or (2 0 0) of the monoclinic phase. The peaks of the tetragonal/cubic phases of the zirconia are no longer visible after annealing at $T = 1223$ K, being substituted by a clear pattern corresponding to the monoclinic phase. The diffraction peaks of this phase are also much narrower now (cf. Table 2), having a full width at half maximum (FWHM) similar to that of the peaks of the (O_2^+)-ZrO_2 thin films reported in Fig. 2 (cf. Table 1). After annealing at 1323 K, a diffraction diagram similar to that depicted by the O_2^+-ZrO_2 sample annealed at the same temperature was obtained.

Fourier transform infrared spectroscopy (FTIR) spectroscopy can be used as a complement of XRD for a more accurate description of the structure of ZrO_2 thin films. Although FTIR is normally used on a "fingerprint" basis, a systematic analysis of IR spectra may also provide insight into the ZrO_2 thin film structure [25–29].

Fig. 4 shows FTIR spectra for the (O_2^+)-ZrO_2 sample as prepared and after different annealing treatments up to 1323 K. Initially, the FTIR spectra of the as prepared O_2^+-ZrO_2 film is characterised by a structure where some broad bands are defined at ≈340, 407 and 490 cm^{-1}. These bands can be attributed to some of the 15 vibrational modes of the monoclinic phase of ZrO_2 [30]. By annealing at $T \leqslant 773$ K, the bands become slightly sharper and increase in intensity. This tendency is even clearer after annealing $T \geqslant 1223$ K, while some new bands centred at ≈258, 460 and 570 cm^{-1} develop in the spectrum. These bands can be also assigned to some of the 15 vibrational modes of the monoclinic phase of ZrO_2 [30]. The increase in intensity at $T \geqslant 1073$K, the development of new bands and the smaller width of the observed bands above this temperature are facts which are consistent with the observed increase in the crystallinity of the monoclinic phase. This tendency can be also deduced from the decrease of

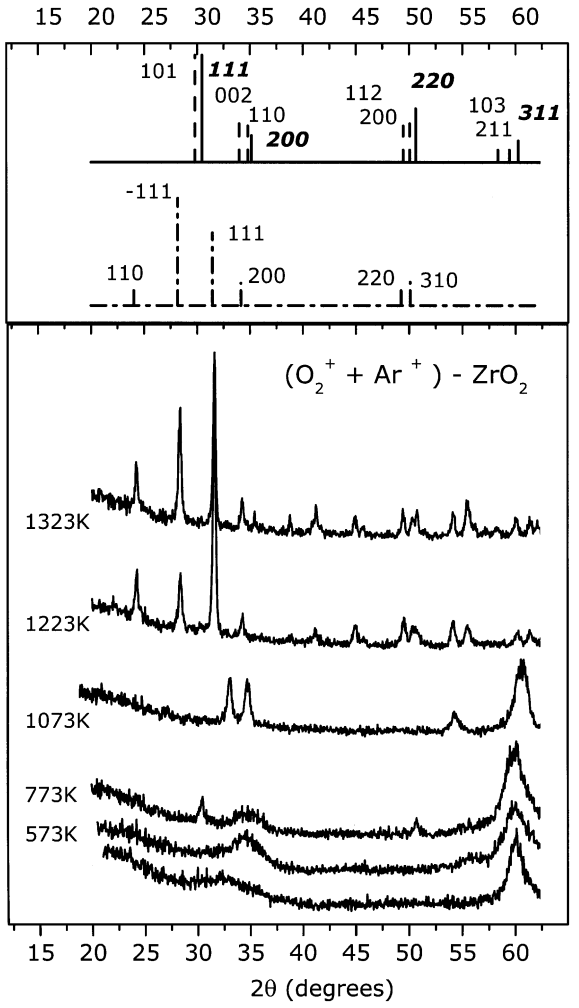

Fig. 3. XRD patterns of $(O_2^+ + Ar^+)$-ZrO_2 thin film for the as prepared samples and after annealing treatments at indicated temperatures. The patterns of the most intense peaks of monoclinic (bottom), cubic (top, full line) and tetragonal (top, dashed line) phases of zirconia are included for comparison.

the FWHM of the peaks of the XRD diagrams presented in Fig. 2 (cf. Table 1).

Fig. 5 shows the FTIR spectra corresponding to a $(O_2^+ + Ar^+)$-ZrO_2 sample subjected to different annealing treatments. The as prepared sample presents only a wide structure with a maximum at $\approx$399 cm^{-1}. After annealing at $T \leqslant 773$ K, this structure becomes slightly sharper and two maxima can be observed at $\approx$343 and 434 cm^{-1}. To our knowledge typical frequencies of the transverse vibrational modes of the cubic or tetragonal phases of pure ZrO_2 are not reported in literature. Therefore, comparison is made with the vibrational frequencies of the cubic and tetragonal phases of Yttria-stabilised ZrO_2 [31] reported in Table 3. Assuming that the presence of yttria might produce some shifts in the position of bands, the spectra in Fig. 5 after annealing at $T \geqslant 573$ K could be consistent with the formation of the tetragonal phase. By contrast, the broad band at $\sim$399 cm^{-1} found in the as prepared sample, could be attributed to a badly ordered cubic and/or tetragonal phase. The broad shapes of all these spectra make it difficult to discard some minority contribution of a cubic phase after annealing at 573 or 773 K. The FTIR spectra of the $(O_2^+ + Ar^+)$-ZrO_2 samples annealed at $T \geqslant 1073$ K undergo drastic changes. The shape of spectra is better defined, and shows bands centred at $\approx$330, 405 and 490 cm^{-1}. The position of these new bands is similar to those that were ascribed to the monoclinic phase of zirconia observed in the (O_2^+)-ZrO_2 samples. However, the superposition of the broad IR structure of the tetragonal phase cannot be discarded in these spectra. It is interesting that no clear evidence of the presence of the monoclinic phase can be deduced from the XRD pattern only of the $(O_2^+ + Ar^+)$-ZrO_2 sample annealed at this temperature (cf. Fig. 2). The different long range order sensitivity of XRD and IR is likely the reason of the different information provided by these two techniques and indicate the advantage of using both methods for a proper evaluation of the structure of some thin films. After annealing at $T = 1323$ K, the bands increase in intensity and become better defined, while some other bands at $\approx$258, 340, 407, 460, 490 and 570 cm^{-1} become also visible. At this final temperature, the spectrum is almost identical to that obtained for the (O_2^+)-ZrO_2 sample annealed at the same temperature.

3.3. Positron annihilation experiments

The *S*-parameter versus implantation energy in the as prepared samples of $(O_2^+ + Ar^+)$-ZrO_2 and (O_2^+)-ZrO_2 series is plotted in Fig. 6(a). Both samples present almost identical variation of this

Table 2
Normalised intensity, referred to most intense peak of each phase and FWHM (in brackets) of the most significant peaks appearing in XRD diagrams of Fig. 3 for $(Ar^+ + O_2^+)$-ZrO_2 samples after indicated annealing treatments

Temperature	Monoclinic			Cubic/tetragonal		
	(1 1 0)	(−1 1 1)	(1 1 1)	(1 1 1)	(2 2 0)	(3 1 1)
300 K	–	–	–	–	–	100 (2.56)
573 K	–	–	–	–	–	100 (2.56)
773 K	–	–	–	–	–	100 (2.10)
1073 K	–	–	–	–	–	100 (1.22)
1223 K	18 (0.29)	21 (0.32)	100 (0.26)	–	–	–
1323 K	25 (0.23)	64 (0.29)	100 (0.23)	–	–	–
Single crystal	25	100	70	100	50	20

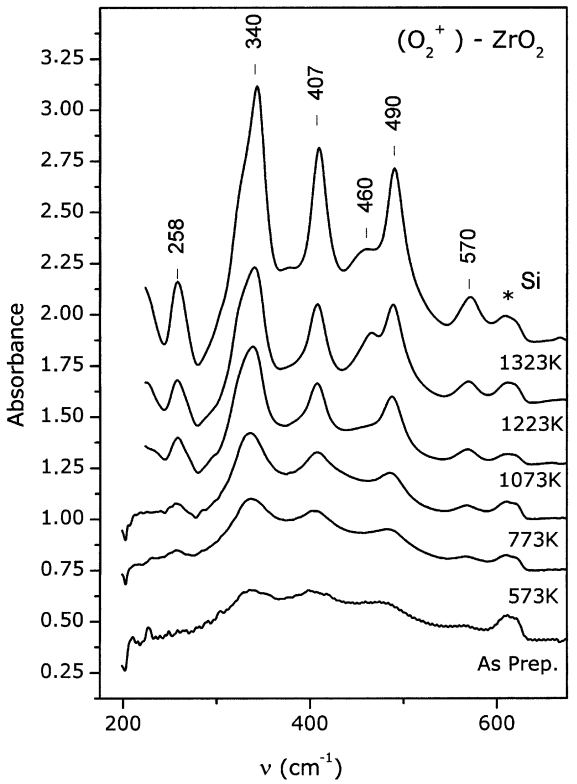

Fig. 4. FTIR spectra of the (O_2^+)-ZrO_2 thin film for the as prepared sample and those obtained after annealing treatments at indicated temperatures.

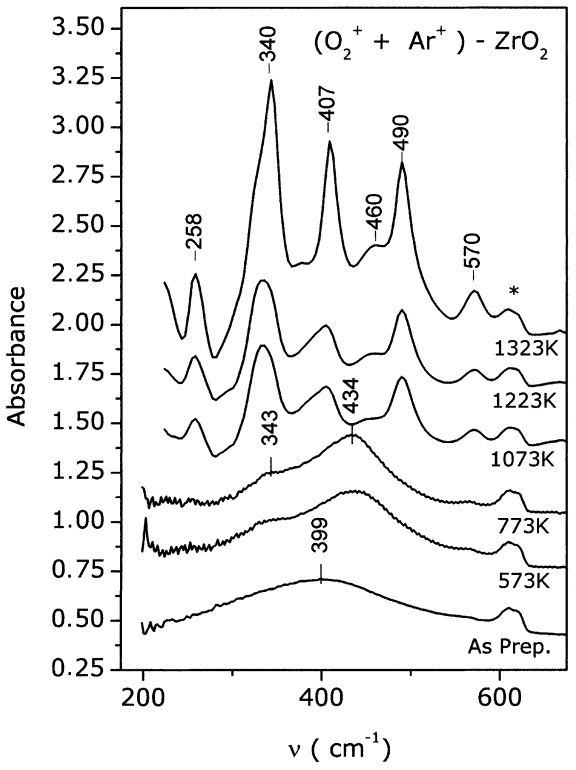

Fig. 5. FTIR spectra of the $(Ar^+ + O_2^+)$-ZrO_2 thin film for the as prepared sample and those obtained after annealing treatments at indicated temperatures.

parameter, indicating that the fraction of open volume in the samples is very similar. By contrast, the variation of the *W*-parameter, presented in Fig. 6(b), shows some differences between the as prepared samples of $(O_2^+ + Ar^+)$-ZrO_2 and (O_2^+)-ZrO_2. In principle, this change can be ascribed to the positron annihilation in the vicinity of argon ions, as they are heavier than oxygen ions and, accordingly, positron annihilation with its core electrons would be enhanced.

Table 3
Some of the IR vibrational modes for tetragonal and Yttria stabilised cubic ZrO_2 (taken from [30])

Phase	v_T (cm^{-1})
Tetragonal	467
	339
Yttria-stabilised cubic	358

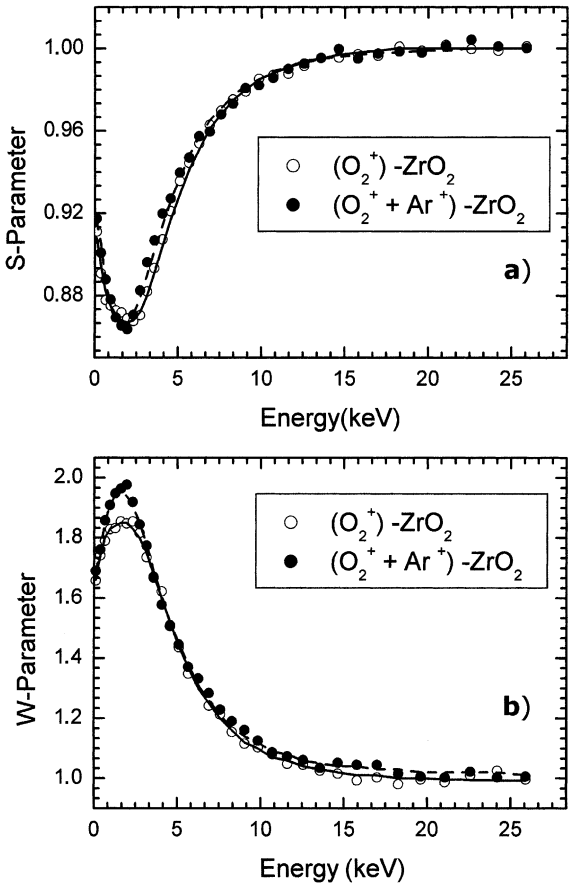

Fig. 6. Variation versus energy of implantation in the as prepared sample of $(O_2^+ + Ar^+)$-ZrO_2 and (O_2^+)-ZrO_2 thin films (a) of the S-parameter (b) of the W-parameter. The lines indicate the fitted values obtained from VEPFIT.

Although the variation of S and W parameters reflects the properties of the samples, a simultaneous representation of these two parameters in S–W plot is usually preferred for a clearer description of the evolution of the thin film properties. Fig. 7 presents the S–W map for the as prepared

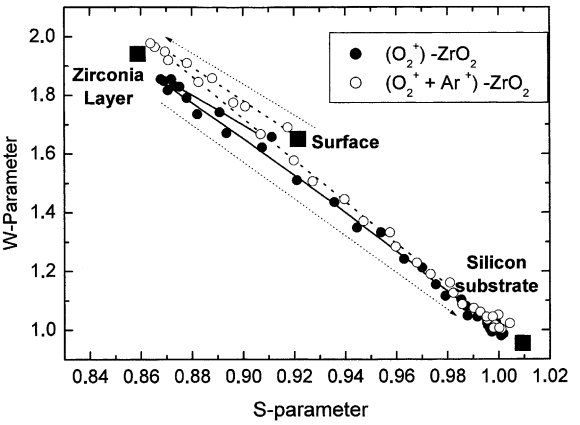

Fig. 7. S–W plot for the as prepared $(O_2^+ + Ar^+)$-ZrO_2 and (O_2^+)-ZrO_2 as prepared, indicating the three-layer system (surface/zirconia layer/silicon substrate). The arrows indicate the positron implantation depth.

$(O_2^+ + Ar^+)$-ZrO_2 and (O_2^+)-ZrO_2 samples. In this kind of plots, information is obtained for the different layers of which the sample is composed. In the current study a three-layer system (surface/zirconia layer/silicon substrate) was applied. As expected, the S–W cluster points of the surface and the silicon substrate are identical in both samples but different in those of the zirconia layer. Thus, changes in the cluster points of the zirconia layer will reflect changes in the structure of the film. The variation of the fitted S–W points corresponding to the zirconia layer for samples of $(O_2^+ + Ar^+)$-ZrO_2 and (O_2^+)-ZrO_2 after annealing treatments at different temperatures is shown in Fig. 8. In Fig. 9 the fitted S and W parameters of the zirconia layer are plotted independently versus the annealing temperature. In both figures for the different sets of samples two annealing stages can be considered: annealing from room temperature to 773 K and annealing above that temperature. In the first case, the S–W characteristic points move to higher S values while the W parameter decreases. Changes in the positron diffusion length were also observed. In fact, for the (O_2^+)-ZrO_2 samples, the positron diffusion length increases from 7.5 nm in the as prepared sample, to 50 nm after annealing at 773 K. For the as prepared $(O_2^+ + Ar^+)$-ZrO_2 sample a shorter positron diffusion length was measured ($\sim$3 nm) and it remains shorter after annealing at

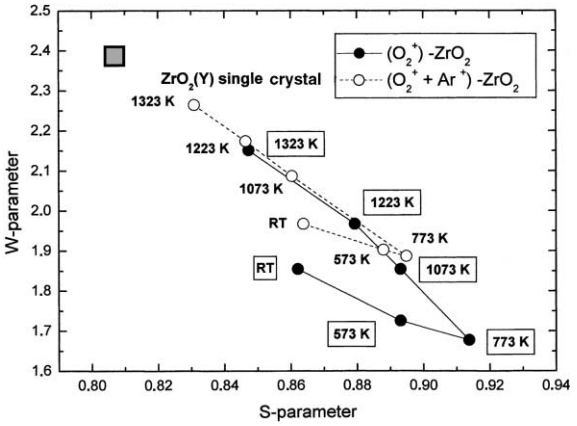

Fig. 8. Variation of the fitted S–W points corresponding to the zirconia layer for as prepared $(O_2^+ + Ar^+)$-ZrO_2 and (O_2^+)-ZrO_2 thin films and the corresponding to those samples after annealing treatments at indicated temperature.

773 K (≈10 nm). The short diffusion lengths measured for the as prepared samples could be related with an initial amorphous state (partially) of the samples. It is likely that the difference between the two samples and the evolution upon annealing up to 773 K are due to roughening processes that, based on AFM data, have been previously reported to occur at the surface of these samples [18]. However, after annealing at $T > 773$ K it is observed that the cluster points in the S–W diagram of the two samples move towards positions with high W and low S values. This tendency is consistent with the progressive increase in crystallinity observed by XRD for the two samples after annealing at $T > 873$ K. It is also interesting that at the highest annealing temperature the positions of the cluster points of the two samples approach each other, a fact that can be related with the progressive loss of Ar from the annealed $(O_2^+$–$Ar^+)$-ZrO_2 samples. In Fig. 8, the cluster point corresponding to a single crystal Y-doped tetragonal zirconia has been included for comparison. With respect to this reference point, those of the ZrO_2 thin films are slightly shifted towards low W and high S values. The monoclinic phase stabilised in the thin films after annealing and, likely, grain boundaries effects are factors contributing to the observed shifts.

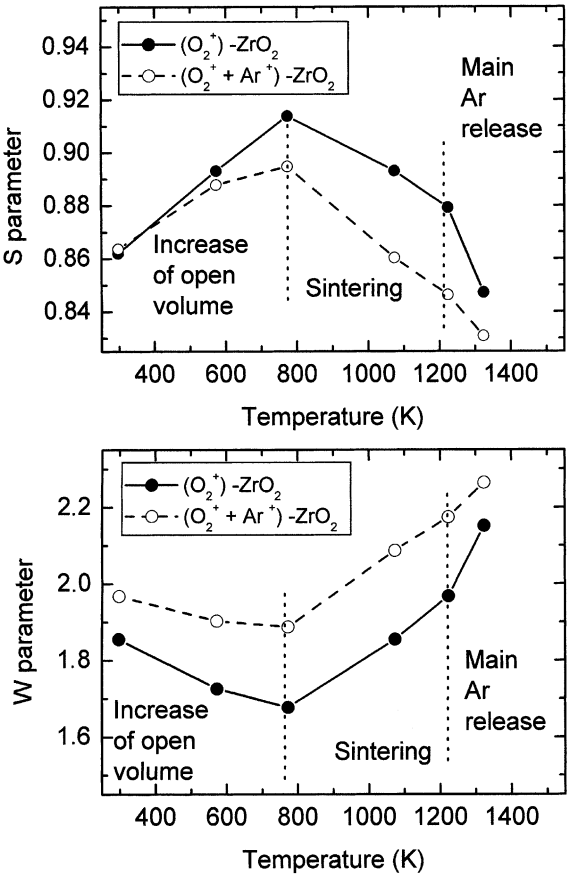

Fig. 9. Variation versus annealing temperature in the $(O_2^+ + Ar^+)$-ZrO_2 and (O_2^+)-ZrO_2 thin films (a) of the fitted S-parameter (b) of the fitted W-parameter.

4. Discussion

RBS analysis of samples has shown that in $(O_2 + Ar^+)$-ZrO_2 thin films a significant amount of Ar (~5–6 at.%) remains homogeneously dispersed within the thin film. The fact that the Ar distribution is not modified by annealing at 773 K suggests a restricted mobility for this atom within the ZrO_2 lattice and/or grain boundaries. Release of Ar starts at $T \geqslant 1023$ K, a temperature at which it is known that the oxygen ion mobility through the ZrO_2 lattice acquires significant values [5,32]. Therefore it is reasonable to assume that mobilisation of oxygen anions by heating may provide the necessary pathways for an effective release of

the embedded Ar atoms. However, total removal of Ar does not occur even after annealing at 1323 K, a fact that supports an effective trapping of this atom within the Zr–O lattice, probably by agglomeration in small argon vacancy complexes.

Incorporation of Ar within the ZrO_2 thin film causes significant modifications in its crystallographic structure. Previous papers in literature on the effect of ion bombardment in ZrO_2 bulk [17] and thin film [16] materials have reported about monoclinic-cubic/tetragonal phase transformation or crystallisation processes from an amorphous state when this material is bombarded with energetic Ar beams. However, in these papers, although implantation of Ar^+ ions within the network is implicitly assumed, a precise study about the fate of these implanted ions and/or their influence on the crystallographic transformations is missing. From the point of view of the energy released after the impingement of the ions onto the growing ZrO_2 thin films prepared with our method, both set of samples, O_2^+-ZrO_2 and (O_2^+–Ar^+)-ZrO_2, should have a similar behaviour. In fact, in both cases the preparation of the films is done by using similar ion densities and energies with a beam of either single or majority O_2^+ species (the Ar^+ ion density cannot be separately measured in our experiment but we assume that it is small since in the feed gas of the ion the O_2/Ar ratio was 10:1). Therefore, for the two sets of samples none or negligible differences should exist in the energetic balance due to the ballistic interactions during the preparation of the films. Therefore, the distinct crystallographic characteristics of the ($O_2^+ + Ar^+$)-ZrO_2 samples should be associated with the incorporation of Ar within the thin film. As deduced from the XRD and FTIR analysis of the structure of the films the features of this study can be summarised as follows:

(a) Ar incorporation produces some amorphisation of the original thin films.
(b) Annealing of samples with embedded Ar at $T < 773$ K stabilises the cubic/tetragonal phases of ZrO_2 with a preferential growth of crystal planes with high Miller indexes (i.e. (3 1 1) of the cubic and/or (2 1 1) of the tetragonal phases in our case).
(c) Annealing at $T = 1023$ K yields a zirconia sample where a distorted cubic/tetragonal phase is detected by XRD while FTIR reveals that the monoclinic structure of zirconia starts to form.

Amorphisation of the as prepared ZrO_2 thin films (i.e. point a) can be considered a general feature of oxide thin films prepared by IBICVD. However, it is remarkable that the amorphisation degree is larger in samples ($O_2^+ + Ar^+$)-ZrO_2 than in O_2^+-ZrO_2 samples. This is an expected behaviour due structural distortions produced by the incorporation of Ar atoms within the ZrO_2 lattice. A similar effect has been observed for Fe_2O_3 thin films prepared by IBICVD with a mixture of Ar^+ and O_2^+ ions [25,33].

It is still unclear what is the cause that produce the stabilisation of the cubic/tetragonal phase of ZrO_2 when Ar is embedded within the lattice (point b). Under thermodynamic equilibrium the transformation of the monoclinic into the tetragonal phase of pure ZrO_2 only occurs at $T > 1446$ K. Therefore, the crystallisation into the tetragonal phase of the ($Ar^+ + O_2^+$)-ZrO_2 thin films at $T \leqslant 773$ K must be due to some effect of the embedded Ar atoms. It is likely that embedded argon leads to an increase of the compressive stress in the films. Stabilisation of the tetragonal or cubic phases of ZrO_2 by the incorporation of defects within its lattice has been recently reported by Sickafus et al. [34]. Stabilisation of the cubic or tetragonal phases of ZrO_2 has been also reported when the constituent particles have a small size ($d \sim 300$ Å) [7]. In our case, although a particle size effect cannot be discarded, the fact that stabilisation of a pure cubic/tetragonal phase is not found for samples O_2^+-ZrO_2 suggests that the main cause leading to the stabilisation of these phases is the incorporation of Ar within the thin film. As mentioned before, increase of lattice stress, generation of defects and other related phenomena must occur by the incorporation of Ar during preparation of the films. Some of these effects have been claimed to account for by the stabilisation of the tetragonal phase in ion doped zirconia [6] and therefore they could have a similar influence here. The high texturing of the films developing crystal

planes with high-Miller indexes (i.e. (3 1 1) of the cubic phase, see Fig. 3) is another effect of the incorporation of Ar within the ZrO_2 lattice that has been also reported for other thin film oxides [25,33]. At present, additional information about the fate of Ar within the lattice would be necessary to formulate a reasonable hypothesis to explain such texturing phenomena.

Removal of some Ar by annealing at $T \geqslant 1073$ K leads to the stabilisation of the monoclinic phase of ZrO_2. An interesting turning point is 1073 K. At this temperature the Ar concentration diminishes to 3% and a mixture of the cubic/tetragonal phase, detected by XRD (cf. Fig. 3) and the monoclinic phase, detected by FTIR (cf. Fig. 5) is found for this sample. The different information provided by the two techniques is not contradictory because of the different length of coherent domains required to yield XRD peaks or FTIR bands. In the second case the existence of local order extending to a limited number of atom shells is enough to produce the bands. In this way, the bands detected after annealing at 1073 K constitute a trace of the crystal nuclei of the monoclinic phase developed at higher annealing temperature (cf. Fig. 5) that are then detected by both XRD and FTIR.

Positron annihilation experiments have revealed the incorporation of Ar in the ZrO_2 films because of the observed changes in the W parameter (Fig. 6). Very short positron diffusion lengths have been found for the as prepared layers indicating an amorphous initial state. The positron diffusion length is shorter in the case of the $(Ar^+ + O_2^+)$-ZrO_2 samples than in the (O_2^+)-ZrO_2 samples. This is consistent with a larger amorphisation degree of the $(Ar^+ + O_2^+)$-ZrO_2 samples as mentioned above.

S–W maps (Fig. 8) and plots of S and W versus annealing temperature (Fig. 9) have been used to monitor the defect structure of the films during annealing. Two different stages were detected:

(a) From room temperature to 773 K, an increase of the S parameter is observed in both sets of samples (Fig. 9(a)). This is related to an increase of the open volume in the samples. This increase is smaller in the samples with embedded Ar, indicating that the trapping centres are filled with the Ar gas. The W parameter decreases (Fig. 9(b)) but it is always higher for the $(Ar^+ + O_2^+)$-ZrO_2 samples than for the (O_2^+)-ZrO_2 samples, reflecting the incorporation of heavier argon ions.

(b) After 773 K a progressive crystallisation of the samples is observed. The open volume decreases with temperature, as shown in Fig. 9(a). The $(Ar^+ + O_2^+)$-ZrO_2 samples always present a lower open volume fraction and the S–W cluster points (Fig. 8) approach the values of an Y-doped zirconia single crystal. It is remarkable that after 773 K, the cluster points lie on a straight line pointing towards the single crystal value. This suggest that there is only one type of defect that are annealed out during sintering. The cluster points for the (O_2^+)-ZrO_2 samples also turn to the single crystal value (Fig. 8) but always with a higher S value (Fig. 9(a)). Only at high-annealing temperatures ($T \geqslant 1150$ K), the cluster points are on the same straight line approaching the single crystal value. At these high temperatures the argon atoms starts to release and the cluster points of both type of samples approach each other, indicating a similar final state. It is interesting that after the loss of argon there is no increase of the S parameter in the $(Ar^+ + O_2^+)$-ZrO_2 samples, thus indicating that the sites occupied by the argon atoms have been completely annealed.

5. Conclusions

Incorporation of Ar within the lattice of a ZrO_2 thin film induces modifications in the structure and microstructure of the films. Most significant is the fact that a cubic/tetragonal phase of ZrO_2 can be stabilised by annealing at $T \leqslant 773$ K, a temperature at which Ar is still embedded within the lattice. Similar effects might have produced the structural modifications reported for pure and doped ZrO_2 bulk [16,17] and thin films and other materials subjected to Ar^+ bombardment during or after preparation. The comparison of the structural evolution of O_2^+-ZrO_2 and $(O_2^+ + Ar^+)$-ZrO_2 thin films suggest that ballistic interactions are not the reason for the stabilisation of the cubic/tetragonal phase for the samples prepared with the $(O_2^+ + Ar^+)$ mixture. This paper suggests the pos-

sibility of systematically using noble gas "doping" as a way of controlling the structure and texture development of thin film materials. However, further studies are still necessary for a clear understanding of the origin of the observed crystallographic effects in materials with Ar atoms embedded within their lattice. Understanding of these causes could lead to a systematic use of this technique for a tailored synthesis of thin ceramic films.

Acknowledgements

We want to express our acknowledgement to Spanish Ministry of Science and Technology (Project No. MAT2001-2820) and the Dutch Technology Foundation STW (Project No. GNS 4901) and MULTIMETOX network for its financial support. We also want to thank the CNA (Sevilla) for the RBS measurements.

References

[1] H. Wendel, H. Holzschuh, H. Suhr, G. Erker, S. Dehnicke, M. Mena, Mod. Phys. Lett. B 4 (1990) 1215.
[2] Y. Komatsu, T. Sato, S. Ito, K. Akadi, Thin Solid Films 341 (1999) 132.
[3] K. Izumi, M. Murakami, T. Deguchi, A. Morita, J. Am. Ceram. Soc. 72 (1989) 1465.
[4] G.-Z. Cao, H.W. Brinkman, J. Meijerink, K.J. De Vries, A.J. Burggraaf, J. Am. Ceram. Soc. 76 (1993) 2201.
[5] A.J. Appleby, Energy 7–8 (1996) 521.
[6] H.G. Scott, J. Mat. Sci. 10 (1975) 1527.
[7] B.E. Yoldas, J. Mat. Sci. 21 (1986) 1080.
[8] Y. Matsuzaki, M. Hishinuma, I. Yasuda, Thin Solid Films 340 (1999) 72.
[9] G. García, J. Casado, J. Llibre, J. Cifre, A. Figueras, S. Galí, J. Bassas, Chem. Vapour Depos. 3 (1997) 91.
[10] N. Sonnenberg, A.S. Longo, M.J. Cima, B.P. Chang, K.G. Ressler, P.C. McIntyre, Y.P. Lin, J. Appl. Phys. 74 (1993) 1027.
[11] S.C. Moulzof, Y. Yu, D.J. Frankel, R.J. Lad, J. Vac. Sci. Technol. A 15 (1997) 1211.
[12] G.K. Wolf, Nucl. Instr. and Meth. B 65 (1992) 107.
[13] Y.J. Mao, C.X. Ren, J. Yuan, F. Zhang, X.H. Lin, S.C. Zon, J. Vac. Sci. Technol. A 15 (1997) 2687.
[14] T. Koch, P. Ziemann, Thin Solid Films 303 (1997) 122.
[15] N. Sommemberg, A.S. Longo, M.J. Cima, B.P. Chang, K.G. O'Resiler, P.C. McIntyre, J. Appl. Phys. 74 (1993) 1027.
[16] P.J. Martin, J. Mat. Sci. 21 (1986) 1.
[17] H.M. Naguib, R. Kelly, J. Nucl. Mat. 35 (1970) 293.
[18] J.P. Holgado, J.P. Espinós, F. Yubero, A. Justo, M. Ocaña, J. Benitez, A.R. González-Elipe, Thin Solid Films 377 (2000) 460.
[19] J.P. Espinós, A. Caballero, V.M. Jiménez, J.C. Sánchez-López, L. Contreras, D. Leinen, A.R. González-Elipe, Adv. Mat CVD 3 (1997) 219.
[20] F. Yubero, A. Stabel, A.R. González-Elipe, J. Vac. Sci. Technol. A 16 (1998) 3477.
[21] D. Leinen, A. Caballero, A. Fernández, J.P. Espinós, A. Justo, A.R. González-Elipe, J. Martin, B. Maurin-Perrier, Thin Solid Films 272 (1996) 99.
[22] A. van Veen, J. Trace, Microprobe Tech. 8 (1&2) (1990) 1.
[23] L.R. Doolittle, Nucl. Instr. and Meth. Phys. Res. B9 (1985) 344.
[24] A. van Veen, H. Schut, J. de Vries, R.A. Hakvoort, M.R. IJpma, in: P.J. Schultz, G.R. Massoumi, P.J. Simpson (Eds.), Advanced Institute of Physics, Vol. 218, New York, 1991, p. 171.
[25] A.R. González-Elipe, F. Yubero, J.P. Espinós, A. Caballero, M. Ocaña, J.P. Holgado, J. Morales, Surf. Coat. Technol. 125 (2000) 116.
[26] D.W. Berreman, Phys. Rev. 130 (1963) 2193.
[27] G.L. Bottger, A.L. Geddes, J. Chem. Phys. 46 (1967) 3000.
[28] F. Proix, M. Balkanski, Phys. Stat. Sol. 32 (1969) 119.
[29] J.S. Ahn, H.S. Choi, T.W. Noh, Phys. Rev. B 53 (1996) 10310.
[30] E. Anastassakis, B. Papanicloaou, I.M. Asher, J. Phys. Chem. Solids 36 (1975) 667.
[31] C. Pecharromán, M. Ocaña, C.J. Serna, J. Appl. Phys. 80 (1996) 33479.
[32] J.O'M. Bockris, B.E. Conway, R.E. White (Eds.), Modern Aspects of Electrochemistry, Number 29, Plenum Press, New York, 1996.
[33] F. Yubero, M. Ocaña, A. Caballero, A.R. Gonzalez-Elipe, Acta. Mater. 48 (2000) 4555.
[34] K.E. Sickafus, H. Matze, T. Hartmann, K. Yasuda, J.A. Valdez, P. Chodak, M. Nastasi, R.A. Verrall, J. Nucl. Mater. 274 (1999) 66.